JCTC Journal of Chemical Theory and Computation

Article

pubs.acs.org/JCTC

Real-Time Quantum Dynamics Reveals Complex, Many-Body Interactions in Solvated Nanodroplets

M. Belén Oviedo* and Bryan M. Wong*

Department of Chemical & Environmental Engineering and Materials Science & Engineering Program, University of California, Riverside, Riverside, California 92521, United States

ABSTRACT: Electronic excitations in the liquid phase are surprisingly rich and considerably more complex than either gas-phase or solid-state systems. While the majority of physical and biological processes take place in solvent, our understanding of nonequilibrium excited-state processes in these condensed phase environments remains far from complete. A central and long-standing issue in these solvated environments is the assessment of many-body interactions, particularly when the *entire* system is out of equilibrium and *many* quantum states participate in the overall process. Here we present a microscopic picture of solute−solvent electron dynamics and solvatochromic effects, which we uncover using a new real-time quantum dynamics approach for extremely large solvated nanodroplets. In particular, we find that a complex interplay of quantum interactions underlies our observations of solute−solvent effects, and simple macroscopic solvatochromic shifts can even be qualitatively different at the microscopic molecular level in these systems. By treating both the solvent and the solute on the same footing at a quantum-mechanical level, we demonstrate that the electron dynamics in these systems are surprisingly complex, and the emergence of many-body interactions underlies the dynamics in these solvated systems.

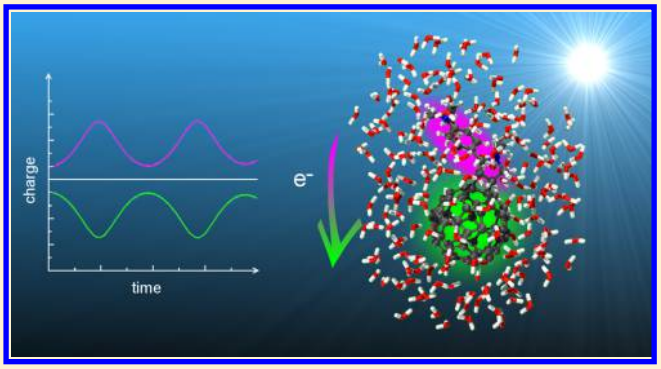

INTRODUCTION

Electronic excitations in the condensed phase play a central role in several fields of scientific research, ranging from light-harvesting chromophores in biochemical systems[1−4] to ultrafast excitations in all facets of time-domain spectroscopy.[5−8] In each of these areas, the physical system exhibits a multitude of interactions (both classical and quantum) between different chemical interfaces that give rise to the experimentally observed spectrum. These many-body interactions are particularly crucial in the liquid phase, as these effects are significantly more complex than in either gas-phase or solid-state systems. While intermolecular interactions are absent in gas-phase systems, and the presence of a lattice creates periodic order in solid-state systems, both of these restrictions are absent in the liquid phase. As such, the interpretation and elucidation of mechanistic details in liquids are inherently complex, and the manifestation of nonequilibrium electron dynamic effects in these systems further adds to their complexity.

A central and long-standing issue in liquid systems is the assessment of many-body quantum effects, particularly when the entire system is out of equilibrium and many quantum states participate in the overall process.[9] While most investigations in the liquid phase (for both theory and experiment) have primarily focused on continuum solvent[10,11] and coarse-grained classical models,[12−14] these approaches often cannot provide satisfactory descriptions of detailed electronic mechanisms in these complex environments. For example, continuum approaches cannot describe detailed solute−solvent interactions at the electronic level and classical models break down considerably when the electronic excitations of the solute are nonperturbative or nonlinear. Notwithstanding these pragmatic issues, on a deeper fundamental level, a more faithful representation of realistic nonequilibrium processes in these systems necessitates the inclusion of both explicit solvent and real-time electronic effects.

Here, we focus on a microscopic picture of solute−solvent electron dynamics and solvatochromic effects, which we uncover using a new real-time quantum dynamics approach for large solvated nanodroplet systems. In particular, we find that a complex interplay of quantum interactions underlies our observations of solute−solvent effects, and simple macroscopic solvatochromic shifts can even be qualitatively different at the microscopic molecular level in these systems. While we focus our studies on a solvated C_{60}:dimethylaniline donor−acceptor nanodroplet for concreteness (C_{60}:dimethylaniline is also utilized in new photovoltaic materials[15,16]), our main qualitative results are expected to apply to a broad range of other solvated donor−acceptor systems. Our ability to probe extremely large systems allows us to highlight the unusual many-body mechanisms that mediate solvatochromic shifts in both nonpolar and polar solvent−without recourse to empirically derived continuum models. Moreover, our time-domain studies

Received: October 27, 2015
Published: February 26, 2016

DOI: 10.1021/acs.jctc.5b01019
J. Chem. Theory Comput. 2016, 12, 1862−1871

of these solvated nanodroplets provide a natural approach to probe in microscopic detail the time-dependent electron dynamics and couplings between the solute and solvent in emergent order. By treating both the solvent and the solute on the same footing at a quantum-mechanical level, we demonstrate that the electron dynamics in these systems are surprisingly rich, and the emergence of many-body interactions underlies the macroscopic solvatochromic shifts in these solvated systems.

REAL-TIME QUANTUM DYNAMICS OF LARGE SYSTEMS

To address the massive sizes of our solvated nanodroplets (up to 205 explicit solvent molecules and 3,594 orbitals) we carried out our electronic structure calculations using the self-consistent density functional tight-binding (SCC-DFTB) formalism.[17] We briefly summarize the SCC-DFTB formalism here, and a more extensive description of this approach is given in refs 17−22. The DFTB formalism is based on the second order expansion of the Kohn−Sham (KS) total energy, E^{KS}, with respect to fluctuations of the electron density, $n(\mathbf{r}) = n^0(\mathbf{r}) + \delta n(\mathbf{r})$, which can be expressed as

$$E^{KS}[n] = \sum_i^{occ} \langle \Psi_i | \hat{T} + v_H[n^0] + v_{xc}[n^0] + v_{ext} | \Psi_i \rangle - \frac{1}{2}\int d\mathbf{r} v_H[n^0]n^0 + E_{xc}[n^0] - \int d\mathbf{r} v_{xc}[n^0]n^0 + \frac{1}{2}\iint d\mathbf{r}d\mathbf{r}' \left[\frac{1}{|\mathbf{r}-\mathbf{r}'|} + \frac{\delta^2 E_{xc}}{\delta n \delta n'}\bigg|_{n^0}\right]\delta n \delta n' + E_{ZZ} \quad (1)$$

In eq 1, Ψ_i are the Kohn−Sham orbitals, $\hat{T}$ is the kinetic energy operator, v_H is Hartree potential, n^0 is a zeroth-order reference electron density, v_{xc} is the exchange-correlation potential, v_{ext} is the external potential due to the atomic potential, E_{xc} is the exchange-correlation energy, and E_{ZZ} is the nuclear repulsion energy. The first term in eq 1 corresponds to a Kohn−Sham effective Hamiltonian, $\hat{H}^0$, evaluated at the reference density n^0, where the diagonal elements correspond to the Kohn-Sham eigenvalues and the nondiagonal elements are calculated in a two-centered approximation as

$$H^0_{\mu\nu} = \langle \phi_\mu | \hat{T} + v_{eff}[n^0_A + n^0_B] | \phi_\nu \rangle, \qquad \mu \in A, \nu \in B \quad (2)$$

where ϕ_μ forms a minimal Slater-type orbital basis centered on the atomic sites, n^0_A is the reference density of the neutral atom A, and v_{eff} is the effective Kohn−Sham potential. These matrix elements, in addition to the overlap matrix elements, are pretabulated for all pairs of chemical elements, significantly improving the computational efficiency of the DFTB approach. The second-to-last term in eq 1 is defined as E_2, and a multipole expansion of δn_A, while keeping the monopole term, preserves rotational invariance of the total energy (see ref 23 for further details) to yield

$$E_2 = \frac{1}{2}\sum_{AB}^{M} \gamma_{AB}\Delta q_A \Delta q_B \quad (3)$$

γ_{AB} is a function of interatomic separation $\gamma_{AB}(U_A, U_B, |\mathbf{R}_A - \mathbf{R}_B|)$ and interpolates smoothly between onsite interactions with a strength $U_A = \gamma_{AA}$ and the bare Coulomb interaction at large separation (the latter is related to the chemical hardness of the atomic species). The quantity $\Delta q_A = q_A - q^0_A$ is the difference between the charge of the isolated atom q^0_A and the charge q_A obtained via a Mulliken population analysis of atom A in the molecule

$$q_A = \frac{1}{2}\sum_{\mu\in A} (\rho\cdot\mathbf{S} + \mathbf{S}\cdot\rho)_{\mu\mu} \quad (4)$$

$\mathbf{S}$ is the overlap matrix, $\rho_{\mu\nu} = \sum_i c^*_{\mu i} n_i c_{i\nu}$ comprises the one-electron density matrix, n_i are the molecular orbital occupations, and $c_{\mu i}$ are the expansion coefficients of Ψ_i obtained by solving the eigenvalue problem in the atomic orbital basis. Lastly, the terms in eq 1 that depend explicitly on n_0 and E_{ZZ} are grouped into a repulsive term, E_{rep}, that finally yields the following expression for the SCC-DFTB total energy

$$E_{DFTB} = E_0 + E_2 = \sum_i^{occ} \langle \Psi_i | \hat{H}^0 | \Psi_i \rangle + \frac{1}{2}\sum_{AB}^{M} \gamma_{AB}\Delta q_A \Delta q_B + E_{rep} \quad (5)$$

In a similar fashion used to calculate $H^0_{\mu\nu}$, the SCC-DFTB Hamiltonian is given by

$$\hat{H}_{DFTB} = \langle \phi_\mu | \hat{H}^0 | \phi_\nu \rangle + \frac{1}{2} S_{\mu\nu} \sum_K^M (\gamma_{AK} + \gamma_{BK})\Delta q_K \quad (6)$$

Since the DFTB Hamiltonian depends explicitly on the atomic charge, a self-consistent charge (SCC) procedure is used in the SCC-DFTB approach to self-consistently solve eq 6. Our use of the SCC-DFTB formalism is crucial to this study since the immense sizes of our systems *cannot* be routinely probed with conventional DFT/TD-DFT or continuum methods. We utilized the DFTB+ code[24] to compute the Hamiltonian, overlap matrix elements, and the initial single-electron density matrix within the self-consistent SCC-DFTB approach. For the calculations performed here, we have used the *mio-1-1* set of Slater-Koster parameters for the C, O, H, and N atoms.[17]

For our real-time electron dynamics calculations, we implemented and utilized a locally modified real-time, time-dependent DFTB (RT-TDDFTB) code for probing the optical properties in all of our solvated systems. This method is based on the real-time quantum-mechanical propagation of the one electron density matrix in the presence of external time-varying electric fields to obtain the optical response of the system. This formalism has been used to probe the nonequilibrium electron dynamics in several large chemical systems,[25] including photoinjection dynamics in dye-sensitized TiO_2 solar cells[26,27] We carry out our real-time electron dynamics calculations by applying a time-dependent electric field to the initial ground state density matrix, resulting in the Hamiltonian[28] $\hat{\mathbf{H}}(t) = \hat{\mathbf{H}}^0 - \mathbf{E}_0(t)\cdot\hat{\boldsymbol{\mu}}(t)$, where $\mathbf{E}_0(t)$ is the applied electric field, and $\hat{\boldsymbol{\mu}}$ is the dipole moment operator. As we are directly propagating the quantum system in the time-domain, we can choose $\mathbf{E}_0(t)$ to have *any* time-dependent form. For example, if $\mathbf{E}_0(t)$ is a Dirac delta function ($= \mathbf{E}_0\delta(t - t_0)$), this corresponds to an optical absorption spectrum in the frequency domain (obtained after a Fourier transform of the time-evolving dipole moment). However, if we choose $\mathbf{E}_0(t)$ to take the form of a sinusoidal perturbation, it represents a continuous interaction of the system with monochromatic light in the time domain. Both of these different choices give a different but *complementary* view of electron dynamics. This duality is a central theme of this work, and we seamlessly switch between both the time and frequency domains to provide a different

DOI: 10.1021/acs.jctc.5b01019
J. Chem. Theory Comput. 2016, 12, 1862−1871

viewpoint of quantum dynamics in our solvated systems. Upon application of either of these time-dependent fields, the density matrix, $\hat{\boldsymbol{\rho}}$, will evolve according to the Liouville-von Neumann equation of motion which, in the nonorthogonal-DFTB basis, is given by

$$\frac{\partial \hat{\boldsymbol{\rho}}}{\partial t} = \frac{1}{i\hbar}(\mathbf{S}^{-1}\cdot\hat{\mathbf{H}}[\hat{\boldsymbol{\rho}}]\cdot\hat{\boldsymbol{\rho}} - \hat{\boldsymbol{\rho}}\cdot\hat{\mathbf{H}}[\hat{\boldsymbol{\rho}}]\cdot\mathbf{S}^{-1}) \tag{7}$$

where $\hat{\mathbf{H}}$ is the Hamiltonian matrix (which implicitly depends on the density matrix $\hat{\boldsymbol{\rho}}$), $\mathbf{S}^{-1}$ is the inverse of the overlap matrix, and $\hbar$ is Planck's constant. For all of our calculations, we chose a time step integration of 4.84×10^{-3} fs (which minimizes any time-propagation errors in eq 7), and $E_0 = 0.001$ V/Å.

When the applied incident fields are smaller than the internal fields within the matter, the system is found to be in the linear response regime.[29] Under these conditions, the time evolution of the dipole moment operator $\hat{\boldsymbol{\mu}}$ can be expressed as the convolution between the applied electric field perturbation and the response function of the system

$$\langle\hat{\boldsymbol{\mu}}(t)\rangle = \int_0^\infty \boldsymbol{\alpha}(t-\tau)\mathbf{E}(\tau)d\tau \tag{8}$$

where $\mathbf{E}(\tau)$ is the electric field used to induce a perturbation in the system Hamiltonian, and $\boldsymbol{\alpha}(t-\tau)$ is the polarizability tensor. Upon application of the convolution theorem, eq 8 can be expressed in the frequency (ω) domain as $\langle\hat{\boldsymbol{\mu}}(\omega)\rangle = \boldsymbol{\alpha}(\omega)\mathbf{E}(\omega)$. The imaginary part of the average polarizability, $\bar{\alpha}$, is an experimentally measurable quantity related to the photoabsorption cross section[30] by the expression $\sigma(\omega) = 4\pi\omega/c\cdot\mathrm{Im}(\bar{\alpha})$, where c is the speed of light, and $\mathrm{Im}(\bar{\alpha})$ is the imaginary part of the average polarizability.

To calculate the photoinduced electron dynamics in the time domain, we can apply a sinusoidal electric field to the Hamiltonian (i.e., $\hat{\mathbf{H}}(t) = \hat{\mathbf{H}}^0 + \mathbf{E}_0\sin(\omega t)\cdot\hat{\boldsymbol{\mu}}$), with a frequency ω tuned to a specific absorption peak for the system of interest and in the direction of the transition dipole moment. The alignment of the incident electric field with the transition dipole moment is obtained via the diagonalization of the polarizability tensor, where the eigenvector having the largest eigenvalue is associated with the direction of maximum polarization. All simulations were carried out on DFTB+ optimized geometries, and charge transfer dynamics were monitored by calculating the time-evolution of the Mulliken charges for all 3 subsystems: the DMA functional group, the fullerene moiety, and the explicit molecules of solvent. The distinct advantage of our approach is that we directly calculate the electron−hole dynamics in the presence of these nonperturbative, time-dependent fields which *cannot* be achieved by a simple time-evolution propagation of an excited state. This capability allows us to probe the intricate real-time electron dynamics of these complex systems at a level of detail that is beyond the reach of traditional linear-response TDDFT approaches.

RESULTS AND DISCUSSION

Control Experiment on C_{60}:DMA. The molecular structure of C_{60}:dimethylaniline (C_{60}:DMA) optimized within the SCC-DFTB formalism is shown in Figure 1. We have also carried out traditional DFT optimizations of this complex, and all of the geometrical parameters (bond lengths, angles, and dihedrals) are in excellent agreement with our SCC-DFTB optimized structure. Figure 2 shows the computed density of states (DOS) of the C_{60}:DMA complex and the projected DOS of the DMA molecule alone. It is important to note that upon functionalization of C_{60} with DMA, a localized electronic state appears within the bandgap of the fullerene. This specific state is responsible for the new band that appears at lower energies in the absorption spectrum (see Figure 3a) and is directly responsible for the charge-transfer process. It is also interesting to point out that the lowest excitation energy for C_{60} appears at

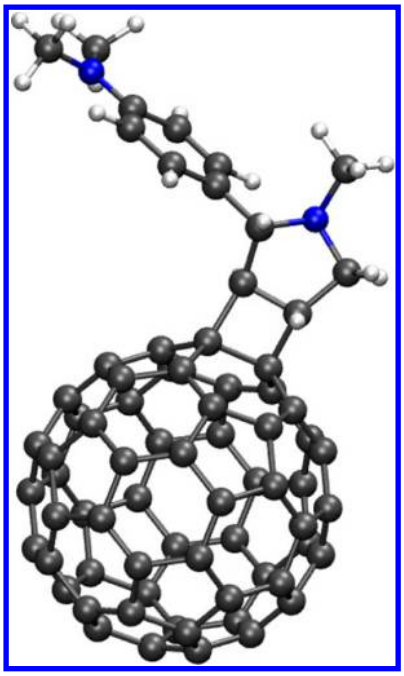

Figure 1. Molecular representation of C_{60}:DMA.

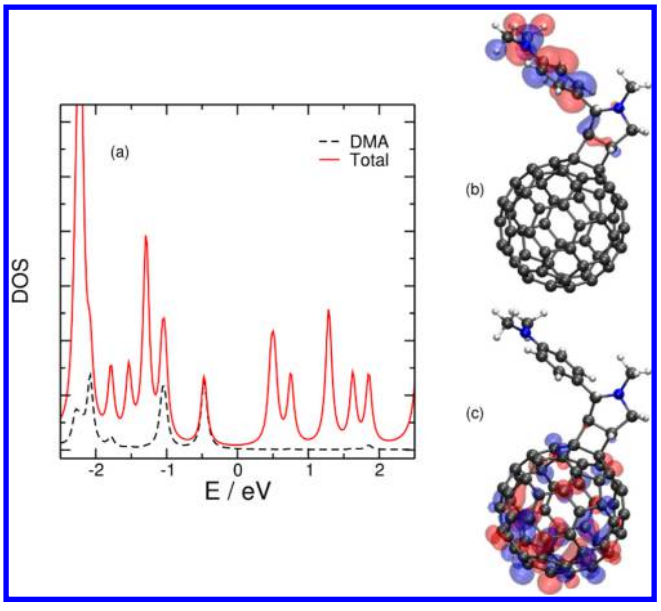

Figure 2. (a) Total density of states (red) and partial density of states projected over the DMA molecule (dashed black line). (b) Highest Occupied Molecular Orbital (HOMO) and (c) Lowest Unoccupied Molecular Orbital (LUMO).

DOI: 10.1021/acs.jctc.5b01019
J. Chem. Theory Comput. 2016, 12, 1862−1871

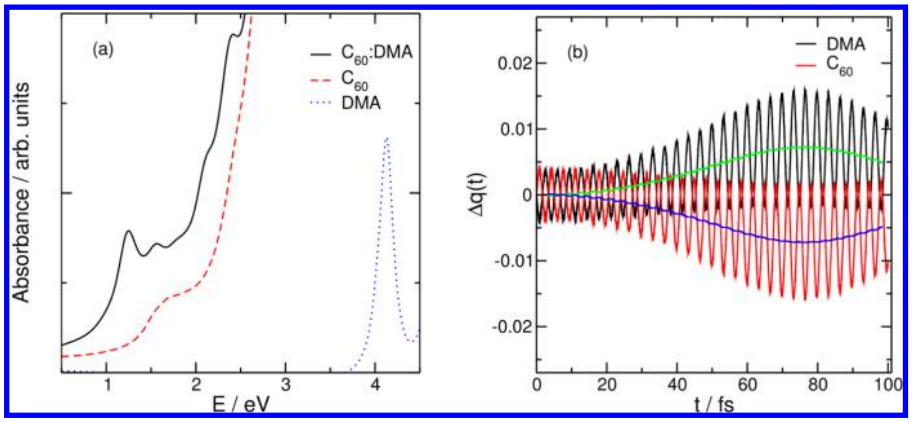

Figure 3. (a) Frequency-domain absorption spectra of C_{60}:DMA, C_{60}, and DMA obtained with RT-TDDFTB. (b) Changes in Mulliken charges with respect to their ground state values as a function of time for both DMA and fullerene. The black line plots the instantaneous charge for DMA, and the red line depicts the instantaneous charge for C_{60}. The green and blue lines plot the average values of the charge for DMA and C_{60}, respectively.

1.7 eV, which corresponds to the optical bandgap of this molecule.

We verified and benchmarked our real-time electronic structure calculations against full linear-response (frequency domain) TDDFT (LR-TDDFT) with the B3LYP hybrid functional. Table 1 summarizes the RT-TDDFTB excitation energies for all of the studied molecular structures. For the DMA, C_{60}, and C_{60}:DMA complexes, all of the RT-TDDFTB excitations agree quantitatively with the full LR-TDDFT calculations. It is also important to note that the initial RT-TDDFTB dipole moment of the C_{60}:DMA complex is 4.13 D, which is in excellent agreement with the full DFT studies by Chapman et al.[31] As such, these benchmarks substantiate the fidelity of the RT-TDDFTB approach and further validate our time-dependent calculations for this system.

Table 1. Comparison of Excitation Energies (eV) in Vacuum Obtained by RT-TDDFTB against Frequency-Domain LR-TDDFT at the B3LYP/6-31+G(d) Level of Theory

	RT-TDDFTB	LR-TDDFT
C_{60}:DMA	1.25	1.32
C_{60}	1.70	1.71
DMA	4.13	4.26

While Figure 3a shows the absorption spectra in the frequency domain, one can obtain additional mechanistic insight by probing the various excitations of the system in the time domain. To further explore the real-time dynamics of this system, we applied a time-dependent sinusoidal electric field to the system with its frequency tuned to the first charge-transfer state in the absorption spectra. As mentioned previously, this frequency corresponds to the new absorption peaks that

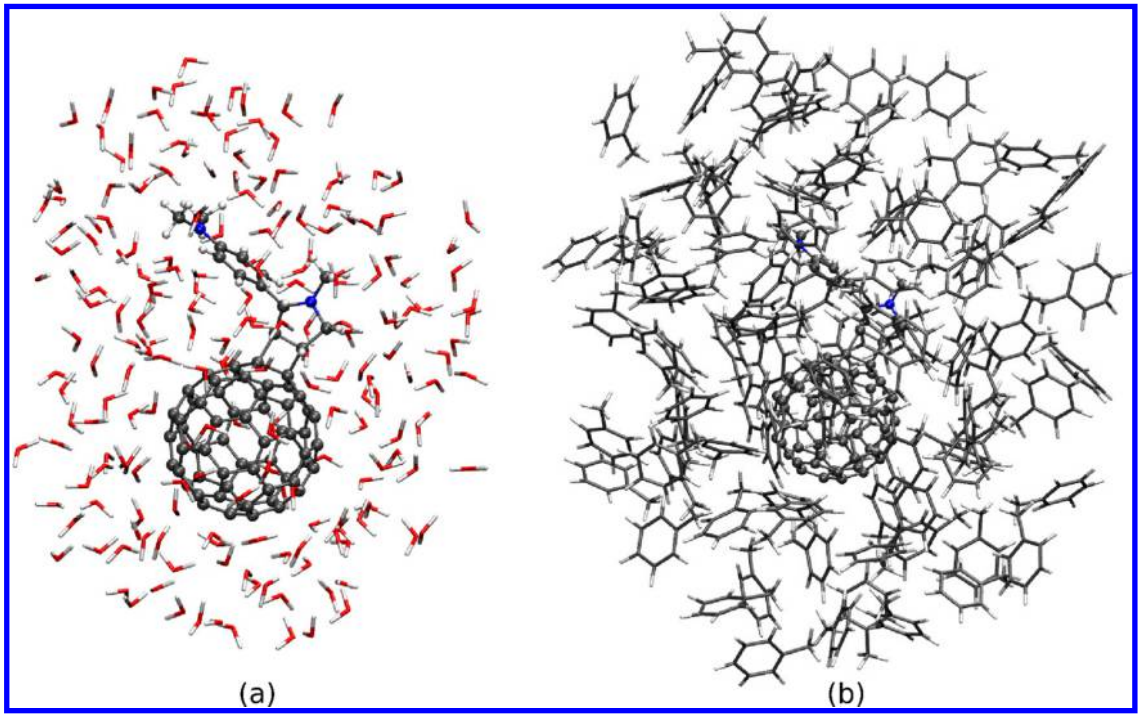

Figure 4. Representative configurations of C_{60}:DMA nanodroplets surrounded by (a) 205 water and (b) 91 toluene explicit solvent molecules.

DOI: 10.1021/acs.jctc.5b01019
J. Chem. Theory Comput. 2016, 12, 1862−1871

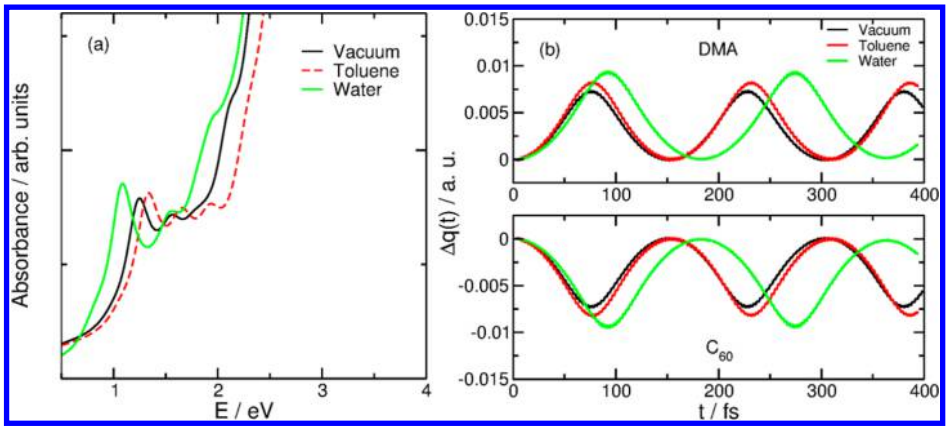

Figure 5. (a) Frequency-domain absorption spectra of C_{60}:DMA in explicit aqueous and toluene solvent. (b) Changes in Mulliken charges as a function of time for both DMA and fullerene in aqueous and toluene solvent.

emerge when the DMA is covalently bonded to the C_{60} acceptor. The polarization direction of the incoming radiation was chosen to align with the transition dipole moment of the entire system. Figure 3b shows the change in the Mulliken charge in both the DMA functional group and the fullerene as a function of time. As can be seen in Figure 3b, there is a net charge transfer from DMA to the C_{60} as the density matrix is propagated in the presence of the time-dependent electric field. These time-dependent calculations provide a complementary perspective of the electron dynamics in C_{60}:DMA obtained in the frequency-domain (cf. Figure 3). We note that the charge-transfer time scales predicted by our calculations are slightly different than the full TDDFT calculations of Chapman[31,32] due to our choice of different system conditions. Specifically, our method is based on the propagation of a density matrix that is *continuously* interacting with a monochromatic field, whereas the work by Chapman[31,32] prepares an excited state by promoting an electron from a selected occupied to an unoccupied molecular orbital. It is important to mention that our method does not take into account phonon-assisted electron-transfer mechanisms. The inclusion of phonons may enhance these charge-transfer process by trapping electrons within the fullerene; however, this is beyond the scope of this work, and most of the quantum physics of the adiabatic charge transfer dynamics is captured by our calculations.

Many-Body Interactions in Solvent. With the electron dynamics of isolated C_{60}:DMA now fully characterized and benchmarked, we now turn to the many-body interactions of this donor−acceptor system in the presence of various complex solvated environments. There have been several prior experimental[33−36] and theoretical studies[37−41] that have demonstrated the importance and complex role of solvent interactions on the optical properties of the solute. As mentioned in the Introduction, while a polarizable-continuum model (PCM) can be used to approximate these solvent effects, the PCM approach becomes inadequate for understanding the detailed solute−solvent dynamics. An alternative approach is to include explicit solvent molecules in solvation shells and perform quantum mechanical calculations on the entire system. However, for large systems, such as the C_{60}:DMA nanodroplet complex studied here, the computational scaling of standard DFT and TDDFT methods increases very steeply with size, resulting in an insurmountable computational cost. As a result, the RT-TDDFTB approach provides a new avenue to calculate these explicit condensed-phase interactions and time-dependent, solute−solvent electron dynamics.

To generate representative solute−solvent nanodroplet geometries (cf. Figure 4) for our electron dynamics studies, we obtained relaxed configurations via a series of molecular dynamics (MD) calculations. It is worth mentioning at this point that the electronic excitations emerging from the explicit application of an electric field (discussed further below) to the entire solute−solvent system are strictly vertical. In other words, solvent relaxation and retardation effects (i.e., Stokes shift spectroscopy) are completely absent in our approach, and no solvent reorganization is assumed to occur during the electronic transitions. Our results arise from the assumption that the solvent is always in equilibrium with the solute throughout the entire electron dynamics. While a full quantum treatment is required to model these important relaxation effects, it is important to note that the inclusion of the time-dependent response of a dielectric medium (TDPCM) to an instantaneous variation of the charge distribution of a molecular system embedded in this dielectric has been recently formulated and implemented with the RT-TDDFT approach in ref 42.

To obtain representative solute−solvent geometries, the solvated C_{60}:DMA complex was placed in a periodic box of side length 55 Å, where the solvent was composed of either 5,590 explicit water or 829 toluene molecules. A short energy minimization of 10,000 (steepest descent) steps was first applied, subsequently followed by a cooling step via a constrained simulated annealing from 400 to 293 K for 1 ns. Finally, a 500 ps NVT (T = 298 K) MD equilibration was carried out with an integration step of 0.2 fs. We used the SPC force-field for the water molecules and the OPLS-AA force-field[43,44] for the toluene molecules. Within these MD simulations, the van der Waals dispersion interactions were approximated by a Lennard-Jones dispersion potential using the UFF parametrization for the van der Waals distance and well depth. While the use of a many-body electronic-structure method is computationally prohibitive in benchmarking these large MD geometries, our intermolecular distances between adjacent solvent molecules are in good agreement with previously studies that investigated small solvated systems with dispersion-corrected functionals,[45] fully nonlocal vdW-based methods,[46] and hybrid DFT methods that also included nuclear quantum effects.[47] For the last configuration of the MD simulation, we selected the nearest 205 molecules of water (91

DOI: 10.1021/acs.jctc.5b01019
J. Chem. Theory Comput. 2016, 12, 1862−1871

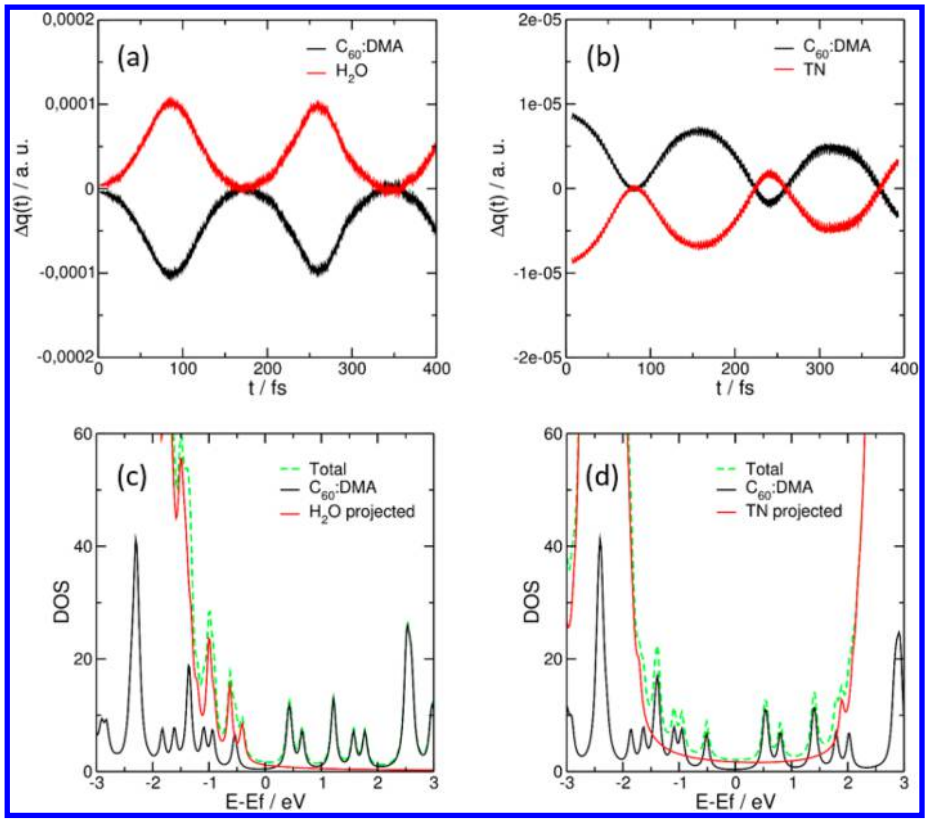

Figure 6. Upper panel: time-dependent Mulliken charge-transfer between C_{60}:DMA and explicit (a) water and (b) toluene molecules in a nanodroplet configuration. The amount of charge-transfer in toluene is an order of magnitude smaller than the electron dynamics in water. Lower panel: projected density of states for C_{60}:DMA and explicit (c) water and (d) toluene molecules.

molecules of toluene) to the C_{60}:DMA complex for the quantum dynamics calculations. We also tried other more complex MD force fields (such as TIP3P and TIP4P) but found that these other MD models had little effect on our real-time electron dynamics calculations or the resulting absorption spectra. It is also important to mention that the main purpose of this work is to probe the many-body interactions to unravel the complex electron dynamics in these nanodroplet systems rather than exploring the immense phase space of MD configurations (which, on average, do not have a dramatic effect on the RT-TDDFTB dynamics).

***Intra*molecular Solute Charge-Transfer Dynamics.** With these relaxed configurations, a series of several RT-TDDFTB calculations were carried out to obtain the absorption spectra of C_{60}:DMA in water and toluene nanodroplets. These series of calculations are summarized in Figure 5a and naturally result in the well-known inhomogeneous broadening of the absorption spectra that can be directly compared to experiment.[48] Indeed, our RT-TDDFTB simulations are in excellent agreement with condensed-phase spectroscopic experiments and show a red-shift of the excitation energies for the polar H_2O solvent relative to vacuum. Conversely, for the nonpolar toluene solvent, we observe a solvatochromic blue shift of the absorption band. It is important to point out that it is computationally prohibitive to obtain these results with conventional Casida-type TDDFT methods due to the immense size of these systems (up to 3,594 orbitals), whereas the entire spectrum can be directly obtained with RT-TDDFTB dynamics. Most importantly, we naturally obtain the solvatochromic shifts and inhomogeneous broadening effects by carrying out our real-time dynamics with *both* the solvent and solute at the quantum-mechanical level.

Similar to our C_{60}:DMA calculations in vacuum, we can obtain additional mechanistic insight by probing the intramolecular excited-state solvent dynamics in the time domain. To probe these effects, we apply a continuous laser perturbation to the entire nanodroplet system with ω tuned to the first charge-transfer excitation. Our resulting time-domain calculations in Figure 5b clearly show that the Mulliken charge dynamics are strongly dependent on the polarity of the solvent. Mechanistically, as the entire nanodoplet interacts with the applied electric field, an electron−hole pair is generated within the C_{60}:DMA complex. This electron−hole pair interacts dynamically with the electrostatic environment of the solvent, resulting in an oscillation period/lifetime that directly increases with solvent polarity (cf. Figure 5b). On a deep mechanistic level, the RT-TDDFTB calculations show that this intramolecular charge-transfer excitation is stabilized by the polar character of the solvent, and recombination of the photoinduced electron−hole pair in aqueous C_{60}:DMA is diminished relative to the nonpolar toluene.

***Inter*molecular Solute−Solvent Charge-Transfer Dynamics.** In addition to intramolecular charge-transfer excitations *within* the C_{60}:DMA nanodroplet complex, we can apply the same real-time quantum techniques to probe intermolecular interactions *between* C_{60}:DMA and the surrounding solvent. These intermolecular dynamics are significantly more complicated as they inherently involve complex many-body interactions throughout the entire system. In other words, the spectrum of the solvated nanodroplet is the result of *collective* electronic excitations acting in concert between the

DOI: 10.1021/acs.jctc.5b01019
J. Chem. Theory Comput. 2016, 12, 1862−1871

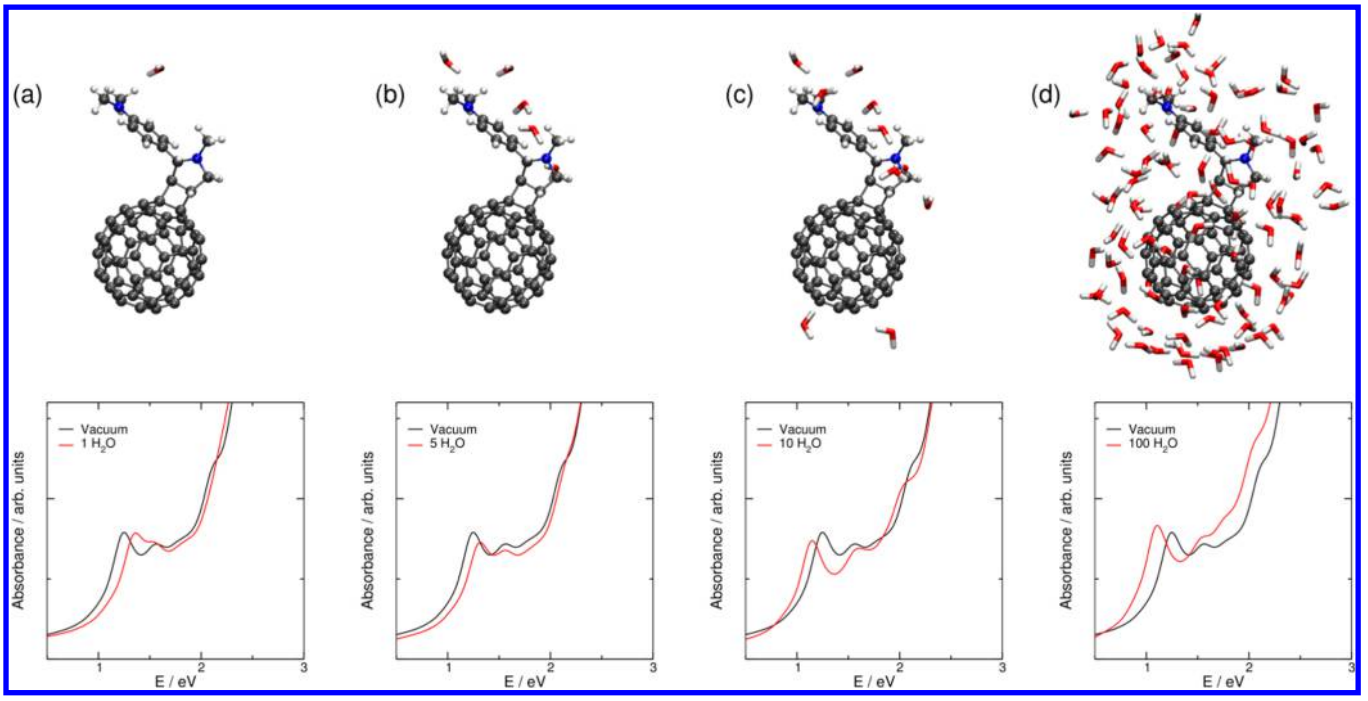

Figure 7. RT-TDDFTB absorption spectra of C_{60}:DMA in the presence of (a) one, (b) five, (c) ten, and (d) one hundred water molecules.

solute and each of the surrounding solvent molecules. To probe these delicate effects, we applied a continuous laser field (with the same charge-transfer excitation frequency used previously) to the entire C_{60}:DMA-solvent system. Figures 6a and 6b show the time-dependent charge fluctuations between C_{60}:DMA and the surrounding water and toluene molecules, respectively. The resulting charge-population analyses clearly show that the dynamics for water and toluene solvent are qualitatively different: in Figure 6a, electron injection from water into C_{60}:DMA occurs, while toluene plays the *opposite* role of the electron acceptor in Figure 6b. Moreover, the amount of charge transferred between toluene and C_{60}:DMA is an order of magnitude smaller compared to the electron dynamics in water.

As before, we can understand these dramatic differences in the time-domain by referring to the corresponding dynamics in the frequency domain. Figures 6c and 6d depict the projected DOS (relative to the Fermi level) for C_{60}:DMA in explicit water and toluene, respectively. In the solvated C_{60}:DMA-water nanodroplet in Figure 6c, we see that the highest occupied molecular orbital (HOMO) of the entire system is localized on the water molecules ($\Delta E = -0.4$ eV). However, the energies of these localized HOMOs lie higher in energy than the HOMO−1 orbitals (located at $\Delta E = -0.6$ eV and localized on the DMA donor group) that are directly involved in the C_{60}:DMA charge-transfer excitation. Consequently, as the laser field interacts with the system, a hole is generated in the HOMO−1 localized on the DMA donor, and an electron is promoted to the unoccupied manifold of states on the C_{60} acceptor. Almost instantaneously, the vacancy left in the HOMO−1 is then refilled by the HOMO electrons from the water, resulting in a net charge-transfer from the solvent to C_{60}:DMA in the time domain (cf. Figure 6a). In contrast, the charge-transfer mechanisms in toluene are markedly different: from Figure 6d, we see that there are no electronic states of toluene in the vicinity of the Fermi level, and the nearest toluene electronic state is an *unoccupied* orbital much higher in energy at $\Delta E = 2$ eV. As a result, when the continuous laser field is applied, we obtain the expected intramolecular charge-transfer excitation between DMA and C_{60}; however, now the unoccupied orbital of toluene plays the role of the electron *acceptor*, resulting in a net transfer of charge from C_{60}:DMA to the solvent instead (cf. Figure 6b). Moreover, since this unoccupied toluene orbital lies much higher in energy, significantly less charge is transferred to toluene compared to water as shown in Figure 6a. It is also interesting to note that we see a noticeable drift in the Mulliken charges for both C_{60}:DMA and toluene in Figure 6b (compared to the stable periodic plot in Figure 6a). This time-dependent drift arises from the larger cross-section of toluene compared to water: the local field generated in the toluene solvent can excite other electron−hole pairs via multipolar coupling which can be subsequently redistributed to other surrounding toluene molecules.

It is important to mention that while all of these charge-transfer processes are a natural outcome of our real-time dynamics approach, *these intricate intermolecular mechanisms (particularly the time-dependent drifts of charge) cannot be obtained from either conventional PCM or simple-point-charge solvent models*. It is also interesting to note that in all of these studies, the applied laser field is tuned to the C_{60}:DMA charge-transfer excitation frequency, which lies outside the absorption window of either the water or toluene solvent. Nevertheless, we *still* observe delicate electron-transfer effects between the solvent and the solute at this excitation frequency which ultimately lead to qualitatively different dynamics in the time domain. Capturing these subtle effects is impossible in either the PCM or simple-point-charge models since the solvent in these methods is treated at a lower level of fidelity, and much of the detailed quantum dynamics between the solvent and solute become irreversibly lost.

A Dynamic, Microscopic Picture of Solvatochromic Shifts. We now turn our attention to unexpected solvatochromic effects that are a direct manifestation of the many-body intermolecular dynamics highlighted previously. These non-intuitive effects are a natural result of the real-time solute−

DOI: 10.1021/acs.jctc.5b01019
J. Chem. Theory Comput. 2016, 12, 1862−1871

solvent electron dynamics and give rise to a new microscopic picture of solvatochromic shifts in these condensed phase systems. To unravel these effects, we further investigated the collective excitations between the individual water solvent molecules and the C_{60}:DMA complex. Figures 7 (a)-(d) show a dramatic variation of the C_{60}:DMA charge-transfer band as the number of surrounding water molecules is sequentially increased. In Figure 7 (a)-(b), we find that the electronic coupling between the few explicit water molecules and the solute gives rise to an overall *blue shift* in the excitation energy of C_{60}:DMA. A priori, one might have instead expected to observe a *red shift* of the spectrum for the polar water solvent, in accordance with conventional solvatochromic principles. However, these macroscopic solute−solvent principles break down at the microscopic level, particularly when the number of solvent molecules become markedly discrete within the nanodroplet. While the Bayliss/Bakshiev theories work well in continuum condensed-phase systems (and even form the basis of the original PCM approach for modeling solvent interactions[49]), we find that these spectroscopic trends are qualitatively different at the molecular level, and our real-time quantum dynamics calculations show strong quantitative and even *opposite* deviations from this rule in these systems.

At the microscopic molecular level, this unexpected blue shift in the excitation energy arises when the individual water molecules are coupled with the DMA functional group. Since the HOMO is localized on the DMA group (cf., Figure 2b), our real-time quantum simulations show that the energy of the HOMO becomes stabilized (i.e., lowered). Conversely, when the individual water molecules are placed near the C_{60} group in Figure 7c, an electronic interaction arises between these solvent molecules and the LUMO of the complex (cf., Figure 2c). In this case, our real-time dynamics simulations reveal that the LUMO becomes stabilized, leading to a red shift of the spectrum. Finally, as we dramatically increase the number of water molecules in Figure 2d, we recover an absorption spectrum that approaches the macroscopic continuum result. Specifically, the continuum result is recovered when at least two solvation shells are included (cf. Figures 5a and 7d); however, this is not a general result, and the number of required solvation shells is expected to be system-dependent on the specific solute and solvent under study. The main features of these systematic, iterative calculations truly highlight the many-body nature of solute−solvent electron dynamics. At the microscopic molecular level, we show that individual solute−solvent interactions lead to a renormalization of the energy levels in the system. As a result, the observed spectrum arises from a complex interplay of energy-level realignments originating from the collective interactions of the discrete solvent with the solute (as well as collective interactions between the solute molecules themselves) in these nanodroplets. Although our discussion initially focused on the interaction of discrete water with the HOMO localized on DMA (which leads to a blue shift in the absorption spectrum), it is also important to mention that the interaction of water with the LUMO (localized on C_{60}) still dominates the absorption spectrum due to the larger surface area of the C_{60} moiety. In other words, the macroscopic absorption spectrum is a measurement of an ensemble of solute−solvent interactions, and the overall spectrum of this system will be red-shifted since the accessible surface area of C_{60} is larger than the DMA surface area. Nevertheless, these collective interactions cannot be gleaned from either continuum or even simple-point-charge models, (whose effects are typically "averaged out"), and the use of atomistic solvent in this work highlights the nonadditive, coherent, many-body nature of solute−solvent electron dynamics in these complex environments.

CONCLUSION

In summary, we have described a detailed computational framework for probing the intrinsic many-bodied nature of solute−solvent electron dynamics in complex solvated nanodroplets. By treating both the solvent and the solute *on the same footing* at a quantum-mechanical level, we demonstrate that the electron dynamics in these solvated systems are surprisingly rich, and macroscopic solvatochromic shifts are even qualitatively different at the molecular level in these systems. The treatment of both the solvent and solute at the same level of theory is crucial since it allows us to elucidate a microscopic picture of these "simple" solvatochromic shifts in condensed phase nanodroplets. Specifically, at the microscopic molecular level, we show that individual solute−solvent interactions lead to a renormalization of the energy levels in the system. Consequently, the observed spectrum is intrinsically due to a complex interplay of energy-level realignments originating from the collective interactions of the discrete solvent with the solute. These realignments are *not additive* or monotonic shifts in energy, and our analysis of the real-time electron dynamics in these nanodroplet systems even show *opposite* deviations at the microscopic molecular level.

Moreover, it is also important to mention that while all of these charge-transfer processes are a natural outcome of our real-time dynamics approach, these intricate intermolecular mechanisms *cannot* be obtained from either continuum or simple-point-charge solvent treatments. By directly probing the real-time electron dynamics in explicit toluene and water solvent (up to 3,594 orbitals), we give crucial insight into the vastly different mechanisms that mediate solvatochromic shifts in both nonpolar and polar solvent—without recourse to empirically derived continuum models. Most notably, we show that the presence of explicit solvent molecules has a nontrivial effect on controlling nonequilibrium charge-transfer processes, as demonstrated by their vastly different time-dependent charge dynamics. Moreover, we find that electron-injection rates from the solvent to the complex have a larger influence on the stabilization dynamics than the opposite mechanism, giving fundamental insight into controlling the electron dynamics of these solvated systems. Capturing these subtle effects is impossible in simple models since the solvent in these minimal methods is treated at a lower level of fidelity, and much of the detailed quantum dynamics between the solvent and solute becomes irreversibly lost. While our treatment recovers the macroscopic spectrum in the limit of large solvent molecules, our real-time electron dynamics approach is essential for unravelling the true many-bodied nature of these "simple" solvatochromic shifts. As such, our real-time dynamics investigations suggest that one way to view solvatochromic effects in general is to regard them as a manifestation of *collective time-dependent* electron dynamics rather than the long-held view of the solvent merely serving as a nondynamic, continuous dielectric environment for the solute.

AUTHOR INFORMATION

Corresponding Authors

*E-mail: maria.oviedo@ucr.edu.

DOI: 10.1021/acs.jctc.5b01019
J. Chem. Theory Comput. 2016, 12, 1862−1871

*E-mail: bryan.wong@ucr.edu. Web: http://www.bmwong-group.com.

Notes

The authors declare no competing financial interest.

■ ACKNOWLEDGMENTS

Support from the National Science Foundation - Institute for Complex Adaptive Matter (NSF-ICAM) is acknowledged. We acknowledge the National Science Foundation for the use of supercomputing resources through the Extreme Science and Engineering Discovery Environment (XSEDE), Project No. TG-CHE140097. We also gratefully acknowledge the support of NVIDIA Corporation with the donation of the Tesla K40 GPU used for this research.

■ REFERENCES

(1) Scholes, G. D.; Fleming, G. R.; Olaya-Castro, A.; van Grondelle, R. Lessons from nature about solar light harvesting. *Nat. Chem.* **2011**, *3*, 763−774.
(2) Fleming, G. R.; Scholes, G. D. Physical chemistry: Quantum mechanics for plants. *Nature* **2004**, *431*, 256−257.
(3) Francesca, F.; Alexandra, O.-C. Distribution of entanglement in light-harvesting complexes and their quantum efficiency. *New J. Phys.* **2010**, *12*, 085006.
(4) Rebentrost, P.; Mohseni, M.; Aspuru-Guzik, A. Role of Quantum Coherence and Environmental Fluctuations in Chromophoric Energy Transport. *J. Phys. Chem. B* **2009**, *113*, 9942−9947.
(5) Albrecht, A. W.; Hybl, J. D.; Faeder, S. M. G.; Jonas, D. M. Experimental distinction between phase shifts and time delays: Implications for femtosecond spectroscopy and coherent control of chemical reactions. *J. Chem. Phys.* **1999**, *111*, 10934−10956.
(6) Abramavicius, D.; Palmieri, B.; Voronine, D. V.; Šanda, F.; Mukamel, S. Coherent Multidimensional Optical Spectroscopy of Excitons in Molecular Aggregates; Quasiparticle versus Supermolecule Perspectives. *Chem. Rev.* **2009**, *109*, 2350−2408.
(7) Milota, F.; Sperling, J.; Nemeth, A.; Mančal, T.; Kauffmann, H. F. Two-Dimensional Electronic Spectroscopy of Molecular Excitons. *Acc. Chem. Res.* **2009**, *42*, 1364−1374.
(8) Gallagher Faeder, S. M.; Jonas, D. M. Two-Dimensional Electronic Correlation and Relaxation Spectra: Theory and Model Calculations. *J. Phys. Chem. A* **1999**, *103*, 10489−10505.
(9) Akimov, A. V.; Prezhdo, O. V. Large-Scale Computations in Chemistry: A Bird's Eye View of a Vibrant Field. *Chem. Rev.* **2015**, *115*, 5797−5890.
(10) Tomasi, J.; Bonaccorsi, R.; Cammi, R.; Delvalle, F. J. O. Theoretical Chemistry in Solution - Some Results and Perspectives of the Continuum Methods and in Particular of the Polarizable Continuum Model. *J. Mol. Struct.: THEOCHEM* **1991**, *234*, 401−424.
(11) Floris, F.; Persico, M.; Tani, A.; Tomasi, J. Ab Initio Effective Pair Potentials for Simulations of the Liquid-State, Based on the Polarizable Continuum Model of the Solvent. *Chem. Phys. Lett.* **1992**, *199*, 518−524.
(12) Delvalle, F. J. O.; Bonaccorsi, R.; Cammi, R.; Tomasi, J. Electron Correlation and Solvation Effects: Part 3. Influence of the Basis Set and the Chemical-Composition on the Solvation Energy Components Evaluated with the Quantum-Mechanical Polarizable Continuum Model. *J. Mol. Struct.: THEOCHEM* **1991**, *230*, 295−312.
(13) Delvalle, F. J. O.; Tomasi, J. Electron Correlation and Solvation Effects: Part 1. Basic Formulation and Preliminary Attempt to Include the Electron Correlation in the Quantum-Mechanical Polarizable Continuum Model So as to Study Solvation Phenomena. *Chem. Phys.* **1991**, *150*, 139−150.
(14) Aguilar, M. A.; Delvalle, F. J. O.; Tomasi, J. Electron Correlation and Solvation Effects: Part 2. The Description of the Vibrational Properties of a Water Molecule in a Dielectric Given by the Application of the Polarizable Continuum Model with Inclusion of Correlation-Effects. *Chem. Phys.* **1991**, *150*, 151−161.
(15) Liu, S.-G.; Shu, L.; Rivera, J.; Liu, H.; Raimundo, J.-M.; Roncali, J.; Gorgues, A.; Echegoyen, L. A New Dyad Based on C_{60} and a Conjugated Dimethylaniline-Substituted Dithienylethylene Donor. *J. Org. Chem.* **1999**, *64*, 4884−4886.
(16) Hasobe, T.; Kamat, P. V.; Absalom, M. A.; Kashiwagi, Y.; Sly, J.; Crossley, M. J.; Hosomizu, K.; Imahori, H.; Fukuzumi, S. Supramolecular Photovoltaic Cells Based on Composite Molecular Nanoclusters: Dendritic Porphyrin and C_{60}, Porphyrin Dimer and C_{60}, and Porphyrin−C_{60} Dyad. *J. Phys. Chem. B* **2004**, *108*, 12865−12872.
(17) Elstner, M.; Porezag, D.; Jungnickel, G.; Elsner, J.; Haugk, M.; Frauenheim, T.; Suhai, S.; Seifert, G. Self-consistent-charge density-functional tight-binding method for simulations of complex materials properties. *Phys. Rev. B: Condens. Matter Mater. Phys.* **1998**, *58*, 7260−7268.
(18) Frauenheim, T.; Seifert, G.; Elstner, M.; Hajnal, Z.; Jungnickel, G.; Porezag, D.; Suhai, S.; Scholz, R. A self-consistent charge density-functional based tight-binding method for predictive materials simulations in physics, chemistry and biology. *Phys. Status Solidi B* **2000**, *217*, 41−62.
(19) Elstner, M.; Seifert, G. Density functional tight binding. *Philos. Trans. R. Soc., A* **2014**, *372*, 20120483.
(20) Cui, Q.; Elstner, M. Density functional tight binding: values of semi-empirical methods in an ab initio era. *Phys. Chem. Chem. Phys.* **2014**, *16*, 14368−14377.
(21) Elstner, M.; Frauenheim, T.; Kaxiras, E.; Seifert, G.; Suhai, S. A self-consistent charge density-functional based tight-binding scheme for large biomolecules. *Phys. Status Solidi B* **2000**, *217*, 357−376.
(22) Elstner, M.; Cui, Q.; Munih, P.; Kaxiras, E.; Frauenheim, T.; Karplus, M. Modeling zinc in biomolecules with the self consistent charge-density functional tight binding (SCC-DFTB) method: Applications to structural and energetic analysis. *J. Comput. Chem.* **2003**, *24*, 565−581.
(23) Foulkes, W. M. C.; Haydock, R. Tight-binding models and density-functional theory. *Phys. Rev. B: Condens. Matter Mater. Phys.* **1989**, *39*, 12520−12536.
(24) Aradi, B.; Hourahine, B.; Frauenheim, T. DFTB+, a Sparse Matrix-Based Implementation of the DFTB Method. *J. Phys. Chem. A* **2007**, *111*, 5678−5684.
(25) Oviedo, M. B.; Negre, C. F. A.; Sanchez, C. G. Dynamical Simulation of the Optical Response of Photosynthetic Pigments. *Phys. Chem. Chem. Phys.* **2010**, *12*, 6706−6711.
(26) Negre, C. F. A.; Fuertes, V. C.; Oviedo, M. B.; Oliva, F. Y.; Sánchez, C. G. Quantum Dynamics of Light-Induced Charge Injection in a Model Dye−Nanoparticle Complex. *J. Phys. Chem. C* **2012**, *116*, 14748−14753.
(27) Oviedo, M. B.; Zarate, X.; Negre, C. F. A.; Schott, E.; Arratia-Pérez, R.; Sánchez, C. G. Quantum Dynamical Simulations as a Tool for Predicting Photoinjection Mechanisms in Dye-Sensitized TiO2 Solar Cells. *J. Phys. Chem. Lett.* **2012**, *3*, 2548−2555.
(28) Yabana, K.; Bertsch, G. F. Time-dependent local-density approximation in real time. *Phys. Rev. B: Condens. Matter Mater. Phys.* **1996**, *54*, 4484−4487.
(29) Mukamel, S. *Principles of nonlinear optical spectroscopy*; Oxford Univ. Press: New York, U.S.A., 1995; p XVIII, 543 S.
(30) Sottile, F. Response functions of semiconductors and insulators: from the Bethe-Salpeter equation to time-dependent density functional theory. Ph.D. Thesis, École polytechnique, Palaiseau, France, 2003.
(31) Chapman, C. T.; Liang, W.; Li, X. Ultrafast Coherent Electron−Hole Separation Dynamics in a Fullerene Derivative. *J. Phys. Chem. Lett.* **2011**, *2*, 1189−1192.
(32) Chapman, C. T.; Liang, W.; Li, X. Solvent Effects on Intramolecular Charge Transfer Dynamics in a Fullerene Derivative. *J. Phys. Chem. A* **2013**, *117*, 2687−2691.
(33) Cai, W.; Wang, M.; Zhang, J.; Wang, E.; Yang, T.; He, C.; Moon, J. S.; Wu, H.; Gong, X.; Cao, Y. Solvent Effect Leading to High Performance of Bulk Heterojunction Polymer Solar Cells by Novel Polysilafluorene Derivatives. *J. Phys. Chem. C* **2011**, *115*, 2314−2319.

DOI: 10.1021/acs.jctc.5b01019
J. Chem. Theory Comput. 2016, 12, 1862−1871

(34) Bansal, S.; Kumar, N. C_{60} and C_{70} Electronic Absorption Spectra in Different Solvents and Matrices. *J. Biomed. Nanotechnol.* **2011**, *7*, 199−201.
(35) Parusel, A. B. J. A semiempirical study for the ground and excited states of free-base and zinc porphyrin−fullerene dyads. *J. Photochem. Photobiol., B* **2000**, *55*, 188−195.
(36) Etzold, F.; Howard, I. A.; Forler, N.; Cho, D. M.; Meister, M.; Mangold, H.; Shu, J.; Hansen, M. R.; Müllen, K.; Laquai, F. The Effect of Solvent Additives on Morphology and Excited-State Dynamics in PCPDTBT:PCBM Photovoltaic Blends. *J. Am. Chem. Soc.* **2012**, *134*, 10569−10583.
(37) Rocha, W. R.; Martins, V. M.; Coutinho, K.; Canuto, S. Solvent effects on the electronic absorption spectrum of formamide studied by a sequential Monte Carlo/quantum mechanical approach. *Theor. Chem. Acc.* **2002**, *108*, 31−37.
(38) Bouř, P. On the influence of the water electrostatic field on the amide group vibrational frequencies. *J. Chem. Phys.* **2004**, *121*, 7545−7548.
(39) Morzan, U. N.; Ramírez, F. F.; Oviedo, M. B.; Sánchez, C. G.; Scherlis, D. A.; Lebrero, M. C. G. Electron dynamics in complex environments with real-time time dependent density functional theory in a QM-MM framework. *J. Chem. Phys.* **2014**, *140*, 164105.
(40) Eilmes, A. Solvatochromic probe in molecular solvents: implicit versus explicit solvent model. *Theor. Chem. Acc.* **2014**, *133*, 1538.
(41) Bistafa, C.; Canuto, S. Solvent effects on the two lowest-lying singlet excited states of 5-fluorouracil. *Theor. Chem. Acc.* **2013**, *132*, 1−10.
(42) Ding, F.; Lingerfelt, D. B.; Mennucci, B.; Li, X. Time-dependent non-equilibrium dielectric response in QM/continuum approaches. *J. Chem. Phys.* **2015**, *142*, 034120.
(43) Jorgensen, W. L.; Maxwell, D. S.; Tirado-Rives, J. Development and Testing of the OPLS All-Atom Force Field on Conformational Energetics and Properties of Organic Liquids. *J. Am. Chem. Soc.* **1996**, *118*, 11225−11236.
(44) Kaminski, G. A.; Friesner, R. A.; Tirado-Rives, J.; Jorgensen, W. L. Evaluation and Reparametrization of the OPLS-AA Force Field for Proteins via Comparison with Accurate Quantum Chemical Calculations on Peptides. *J. Phys. Chem. B* **2001**, *105*, 6474−6487.
(45) Ilawe, N. V.; Raeber, A. E.; Schweitzer-Stenner, R.; Toal, S. E.; Wong, B. M. Assessing backbone solvation effects in the conformational propensities of amino acid residues in unfolded peptides. *Phys. Chem. Chem. Phys.* **2015**, *17*, 24917−24924.
(46) Wang, J.; Román-Pérez, G.; Soler, J. M.; Artacho, E.; Fernández-Serra, M.-V. Density, structure, and dynamics of water: The effect of van der Waals interactions. *J. Chem. Phys.* **2011**, *134*, 024516.
(47) DiStasio, R. A.; Santra, B.; Li, Z.; Wu, X.; Car, R. The individual and collective effects of exact exchange and dispersion interactions on the ab initio structure of liquid water. *J. Chem. Phys.* **2014**, *141*, 084502.
(48) Seabra, G. d. M.; Walker, R. C.; Elstner, M.; Case, D. A.; Roitberg, A. E. Implementation of the SCC-DFTB Method for Hybrid QM/MM Simulations within the Amber Molecular Dynamics Package. *J. Phys. Chem. A* **2007**, *111*, 5655−5664.
(49) Nagae, H. Theory of solvent effects on electronic absorption spectra of rodlike or disklike solute molecules: Frequency shifts. *J. Chem. Phys.* **1997**, *106*, 5159−5170.

DOI: 10.1021/acs.jctc.5b01019
J. Chem. Theory Comput. 2016, 12, 1862−1871